AIP | Applied Physics Letters

Hard X-ray dark-field imaging with incoherent sample illumination

Marco Endrizzi, Paul C. Diemoz, Thomas P. Millard, J. Louise Jones, Robert D. Speller, Ian K. Robinson, and Alessandro Olivo

Citation: Applied Physics Letters **104**, 024106 (2014); doi: 10.1063/1.4861855
View online: http://dx.doi.org/10.1063/1.4861855
View Table of Contents: http://scitation.aip.org/content/aip/journal/apl/104/2?ver=pdfcov
Published by the AIP Publishing

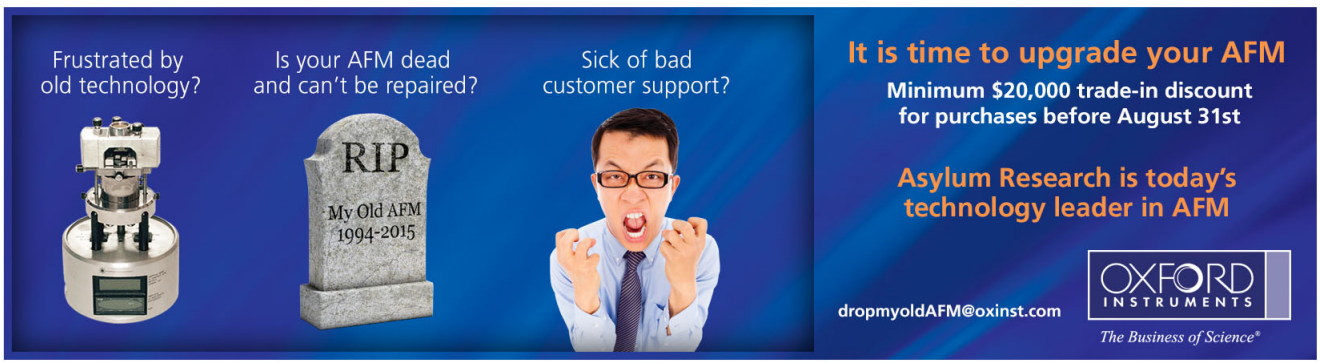

Hard X-ray dark-field imaging with incoherent sample illumination

Marco Endrizzi,[1,a)] Paul C. Diemoz,[1,2] Thomas P. Millard,[1] J. Louise Jones,[3] Robert D. Speller,[1] Ian K. Robinson,[2,4] and Alessandro Olivo[1,2]
[1]*Department of Medical Physics and Bioengineering, University College London, Gower Street, WC1E 6BT London, United Kingdom*
[2]*Research Complex at Harwell, Harwell Oxford Campus, OX11 0FA Didcot, United Kingdom*
[3]*Centre for Tumour Biology, Institute of Cancer, Barts and the London School of Medicine and Dentistry, John Vane Science Centre, Charterhouse Square, EC1M 6BQ London, United Kingdom*
[4]*London Centre for Nanotechnology, WC1H 0AH London, United Kingdom*

(Received 30 October 2013; accepted 28 December 2013; published online 15 January 2014)

We report on a non-interferometric technique enabling dark-field imaging by using incoherent illumination and two achromatic optical elements. The simultaneous retrieval of absorption and differential phase images in the hard X-ray regime is also provided. We show that three projection images are sufficient to separate three signals: absorption, differential phase, and scattering. The method is highly efficient, also in terms of the dose delivered to the sample, flexible, robust against environmental vibrations, and scalable. It can be easily implemented in laboratories and translated into commercial systems, lending itself to a wide range of applications. © *2014 AIP Publishing LLC*. [http://dx.doi.org/10.1063/1.4861855]

Hard X-ray imaging is an invaluable tool in medical, biological, and materials sciences. Enhanced sensitivity can be obtained by means of phase-contrast imaging techniques,[1–10] especially when the samples exhibit weak absorption.[5] An increasing interest has been recorded recently in the so called multi-modal imaging applications.[11–13] Here we show a non-interferometric and incoherent phase-contrast imaging technique based on the edge-illumination principle which, in addition to absorption and refraction,[14,15] enables also the ultra-small-angle scattering retrieval by means of a pair of apertured masks and a rotating anode X-ray tube. The technique does not require spatial or temporal coherence,[16,17] and it is robust against environmental vibrations and thermal stress. The optical elements are achromatic, and the full spectrum is exploited for generating signal at all wavelengths, over which the detector integrates. In our set-up, the coherence length is about 0.5 μm, much smaller than the pitch of about 67 μm of the pre-sample mask, and a large energy spread $\Delta E/\bar{E} \sim 0.7 - 0.3$[17] is typically employed. As we will show in the following, three projection images are sufficient to simultaneously retrieve three quantitative representations of the sample: absorption, differential phase, and (ultra-small-angle) scattering. This last channel, also referred to as dark-field, has been linked to the microscopic structure of the sample on sub-pixel scale lengths, thus yielding complementary information, and methods have been previously demonstrated for measuring it by means of analyser-based and X-ray Talbot imaging.[9,18–22]

The edge illumination principle was first developed at the Elettra synchrotron in Italy in the late nineties.[23] Edge illumination enables the detection of the phase shift, imparted to an X-ray beam traversing a sample, by means of a simple set-up composed of two absorbing slits and a detector. Coded-aperture systems enable its translation to area imaging using conventional rotating anode X-ray tubes.[14,24] Our experimental set-up is composed as follows. A first series of apertures b_1 with period p_1 is placed before the sample (pre-sample mask) and a second series, with aperture b_2 and period p_2, is placed in front of the detector (detector mask). The detector pitch p_3 matches the projected masks' pitches, such that a one-to-one relationship exists between each aperture and the pixel columns of the detector (Fig. 1).

Apertures oriented in the y direction result in sensitivity along x; hence, we deal with a one-dimensional problem in x. The pixels can be considered independent one from the other, as long as the angular spectrum of the beam is limited to $\theta_l < 2p_2/z_{od} \sim 400$ μrad (z_{od} is the sample-to-detector distance). It was previously shown[16,25,26] that geometrical optics can provide a sufficiently accurate description when conventional laboratory sources are used. By using geometrical optics, we were able to obtain analytical inversion formulae for the three representations of the sample. Let us consider $B_1(x) = (1/Gb_1)\mathrm{rect}(x/Gb_1)$ as the detector-plane image of the pre-sample aperture that would be produced by a point source, where rect(x) is the rectangular function defined as 1 for $-1/2 < x < 1/2$ and 0 elsewhere, and G is the geometrical magnification. With a finite source, the image of the pre-sample aperture is given by $B_1 * S$, where * denotes convolution and S is the source distribution projected on the detector plane. The detector pixel integrates this intensity distribution between the limits defined by the detector mask aperture $B_2 = \mathrm{rect}(x/b_2)$. This leads to the illumination function $L(\bar{x}) \equiv (B_1 * S * B_2)(\bar{x})$ that describes how the detected intensity changes as a function of the relative displacement $\bar{x}$ between pre-sample and detector masks. With the sample in place, the intensity $I(\bar{x})$ recorded by the detector pixel can be written as

$$\frac{I(\bar{x})}{I_0} = (B_1 * S * O * B_2)(\bar{x} - \Delta x_R)t, \qquad (1)$$

[a)]Author to whom correspondence should be addressed. Electronic mail: m.endrizzi@ucl.ac.uk

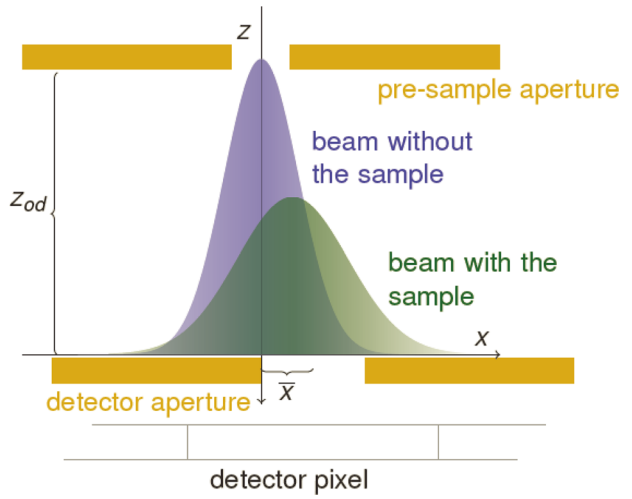

FIG. 1. Beam distribution for a single aperture: the presence of the sample results in an attenuated, shifted, and broadened intensity distribution.

an by exchanging the order of convolutions one obtains

$$\frac{I(\bar{x})}{I_0} = (O * L)(\bar{x} - \Delta x_R)t, \tag{2}$$

where I_0 is the beam intensity passing through the pre-sample aperture and t is the fraction of intensity transmitted through the sample. The detector aperture B_2 appears shifted by $-\Delta x_R = z_{od}\Delta\theta_R$ with respect to the beam as a consequence of the local deflection of the beam by an angle $\Delta\theta_R$, caused by the sample-induced refraction. This angle is directly proportional to the gradient of the phase shift $\Phi(x,y)$ induced by the sample, $\Delta\theta_R = (\lambda/2\pi)(\partial\Phi(x,y)/\partial x)$,[3,27] where λ is the radiation wavelength. The function $O(x)$ describes the scattering (beam broadening) introduced by the sample. This broadening was observed in early experiments with analyser crystals at synchrotrons.[18–20] This effect was also theoretically described, modelled and numerically simulated for various phase-contrast imaging techniques,[28–31] and put in relation with sub-pixel scale inhomogeneities of the sample. We aim to measure this same broadening effect with our laboratory set-up by using incoherent radiation with a large energy spread. Assuming that L and O can be expressed as a linear combination of Gaussian functions, $L(x) = \sum_{n=1}^{N}(A_n/\sqrt{2\pi\sigma_n^2})\exp[-(x-\mu_n)^2/2\sigma_n^2]$ and $O(x) = \sum_{m=1}^{M}(A_m/\sqrt{2\pi\sigma_m^2})\exp[-(x-\mu_m)^2/2\sigma_m^2]$, Eq. (2) can be written in the following form:

$$\frac{I(x)}{I_0} = t\sum_m\sum_n A_{mn}\exp\left[-\frac{(x-\mu_{mn})^2}{2\sigma_{mn}^2}\right], \tag{3}$$

with $\mu_{mn} = \mu_m + \mu_n$, $\sigma_{mn}^2 = \sigma_m^2 + \sigma_n^2$ and $A_{mn} = A_m A_n (1/\sqrt{2\pi\sigma_{mn}^2})$. In the case $N=1$ and $M=1$ (the number of terms in the sums describing $L(x)$ and $O(x)$), let us consider three images acquired with relative displacement of the masks of $x_1 = -x_3$ and $x_2 = 0$. Using Eq. (3), the following system can be written:

$$I_i = t\frac{A_{MN}}{\sqrt{2\pi\sigma_{MN}^2}}\exp\left[-\frac{(x_i - \Delta x_R)^2}{2\sigma_{MN}^2}\right], \quad i = 1,2,3, \tag{4}$$

that can be analytically solved for t, Δx_R and σ_M^2

$$\begin{cases} t = \dfrac{2x_1}{A_{MN}}\sqrt{\dfrac{\pi}{D+C}}I_2\exp\left[\dfrac{1}{2^4}\dfrac{(D-C)^2}{D+C}\right] \\ \Delta x_R = \dfrac{x_1}{2}\dfrac{D-C}{D+C} \\ \sigma_M^2 = \dfrac{2x_1^2}{D+C} - \sigma_N^2, \end{cases} \tag{5}$$

where $C = -2\ln(I_1/I_2)$ and $D = -2\ln(I_3/I_2)$. This allows to separate the contributions to I_1, I_2 and I_3 coming from absorption, refraction and scattering in the sample. For simplicity's sake we are limiting Eq. (3) to the case $N,M=1$; this provides a good approximation for L when extended sources are used and a Gaussian distribution of the scattering, although approximate, has been widely used in the literature.[22] However, if a more complex description must be used, the problem can be tackled by using a larger number of terms in Eq. (3).

The images shown in Fig. 2 were acquired with an amorphous Selenium flat panel (Anrad SMAM) with pixel pitch $p_3 = 85\,\mu$m. The source was a rotating anode, Mo target X-ray tube (Rigaku MM007) operated at 35 kV/25mA and with spot size 75 μm. The masks were manufactured to our design by Creatv Microtech (Potomac, MD) and aligned using a stack of Newport (ILS150, MFA and SR50) and Kohzu (SA07A-RM) stages. The pre-sample mask pitch and aperture were $p_1 = 66.8\,\mu$m and $b_1 = 12\,\mu$m; for the detector mask, they were $p_2 = 83.5\,\mu$m and $b_2 = 20\,\mu$m. For the two offset frames, the masks misalignment $x_1 = 12\,\mu$m was used (Eq. (4)). The gold thickness was approximately 30 μm on a graphite substrate, field of view 4.8×4.8 cm. The source to detector distance was 2 m and the object to detector distance $z_{od} = 40$ cm, for a geometrical magnification factor $G = 1.25$. This parameters were chosen as a trade off between the sensitivity of the system and the dose delivered to the sample.[32] The acrylic cylinders had a diameter of 3 mm and a density of 1.2 g/cm^3. The breast tissue sample was approximately 2 cm thick and fixed in formalin. It was obtained from mastectomy after informed consent; the study was approved by the local ethical regulatory bodies. A filtration of 30 μm of Mo was used in this case. Entrance doses were measured with a calibrated ionization chamber and with TLDs obtaining compatible results within 10%.

As a preliminary demonstration, the extracted images for acrylic cylinders and a paper step wedge are shown in Figs. 2(a)–2(c). In the transmission image (Fig. 2(a)), the three cylinders appear with the same contrast, regardless of their spatial orientation. The refraction image (Fig. 2(b)) shows a strong differential phase contrast for the two vertical cylinders while the horizontal one has a weak signal, except at its vertical edge where the cylinder itself terminates. The presence of the microscopic structure of paper is linked to the signal in the scattering image (Fig. 2(c)). The acrylic, which has negligible density variations at the sub-pixel scale, vanishes. The intensity profiles, along the lines highlighted in Figs. 2(a)–2(c), are plotted in the (g) panel (please refer to the supplemental material[33] for discussion about the efficacy of the method). As an example of a relevant application, the images of a breast tissue

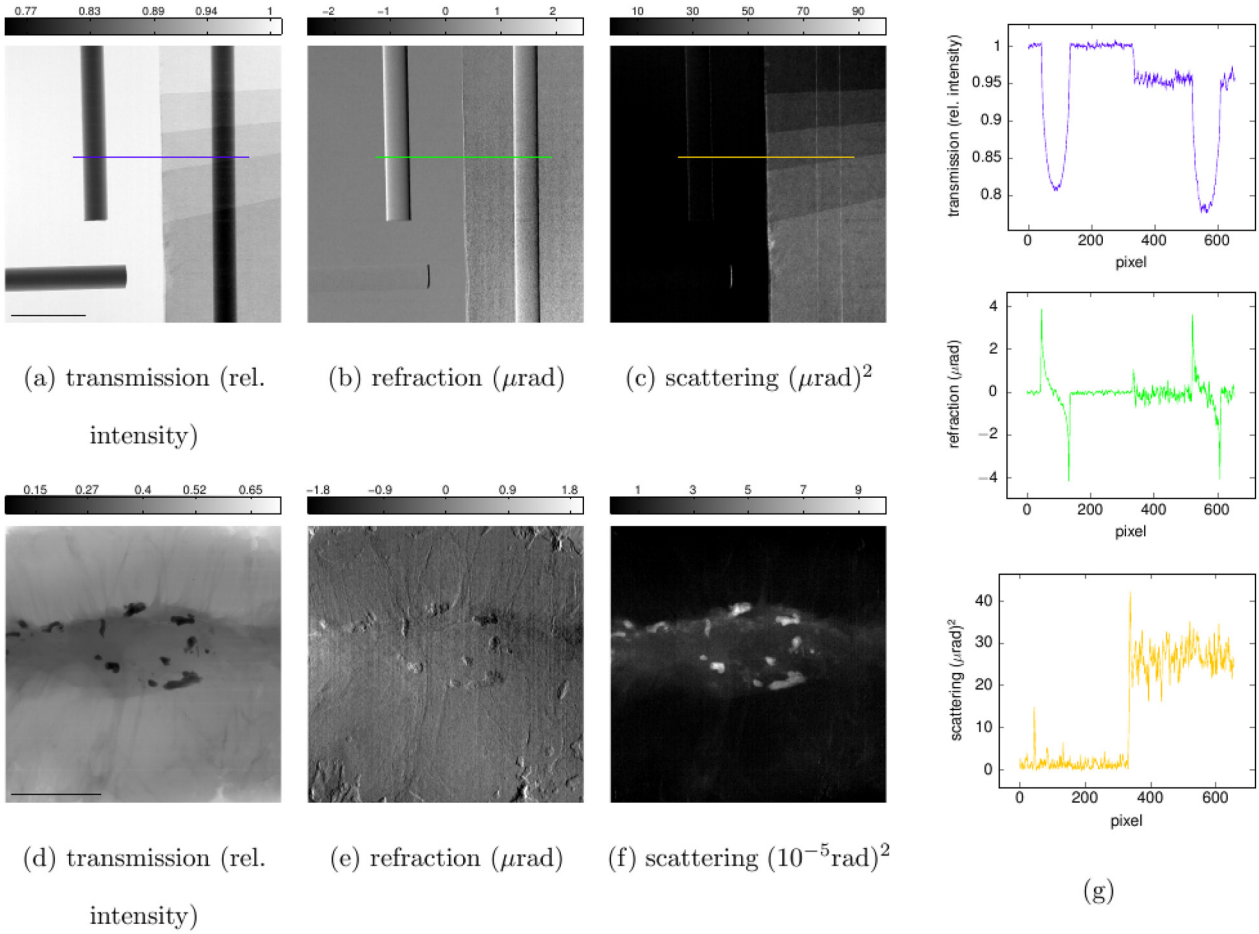

FIG. 2. Demonstrative phantom and biological sample. The images of three acrylic cylinders and a step wedge made of five layers of paper are retrieved using Eq. (5) (scale bar 1 cm): (a) transmission, (b) refraction, and (c) scattering. The corresponding intensity profiles, along the lines highlighted, are plotted in the (g) panel. Images of *ex-vivo* breast tissue sample (scale bar 1 cm): (d) transmission, (e) refraction, and (f) scattering.

sample are also presented: Fig. 2(d) transmission, Fig. 2(e) refraction, and Fig. 2(f) scattering. This sample contains a significant number of calcifications, the contrast inversion of which can clearly be observed by comparing transmission and scattering images. The images were obtained with a surface entrance dose of 12 mGy; although this value appears compatible with the limits imposed by clinical practice,[34] the thickness of the sample has to be taken into account in order to estimate the mean glandular dose that would be required with a full-size breast. With the same photon statistics at the detector and assuming a 4 cm, 50%–50% glandular-adipose breast tissue composition,[32] the estimated mean glandular dose would be about 6 mGy.

In summary, we showed how hard X-ray dark-field imaging can be efficiently performed using a set of two cheap, low-aspect-ratio masks and a rotating anode X-ray tube. The technique uses incoherent illumination and operates with broadband radiation with all wavelengths positively contributing to the image formation. The set-up was realized with standard laboratory instrumentation and it is scalable to larger fields of view. In a commercial device, the second mask could be directly coupled with the detector and the alignment of only one mask would be required. This can be automated[35] yielding even more robustness; we are currently observing vibrations of the experimental set-up of few microns,[36] without this preventing a high image quality. Similar systems have been used at higher energies,[37] and the imaging method proposed here can be straightforwardly applied also with such setups. The ability to span over a wide range of energies gives the method the flexibility required to be useful in a number of different fields. This is of interest for many applications as, for example, security screening,[38] non-destructive testing,[39] cartilage imaging,[13,40] and mammography:[11,41,42] for this last example, we showed experimental images of a breast specimen. Extension to three-dimensional imaging is currently under development in our group. We believe that the robustness of the method and its flexibility to efficiently target specific applications should provide the underpinning technology for mainstream implementations of phase-contrast X-ray imaging.

This work was supported by the UK Engineering and Physical Sciences Research Council (Grant Nos. EP/G004250/1, EP/I022562/1, and EP/I021884/1). M.E. and P.C.D. are supported by Marie Curie Career Integration Grant within the Seventh Framework Programme of the European Union, PCIG12-GA-2012-334056 and PCIG12-GA-2012-333990.

[1]U. Bonse and M. Hart, Appl. Phys. Lett. **7**, 99 (1965).
[2]A. Snigirev, I. Snigireva, V. Kohn, S. Kuznetsov, and I. Schelokov, Rev. Sci. Instrum. **66**, 5486 (1995).

[3]T. J. Davis, D. Gao, T. E. Gureyev, A. W. Stevenson, and S. W. Wilkins, Nature **373**, 595 (1995).
[4]V. N. Ingal and E. A. Beliaevskaya, J. Phys. D **28**, 2314 (1995).
[5]S. W. Wilkins, T. E. Gureyev, D. Gao, A. Pogany, and A. W. Stevenson, Nature **384**, 335 (1996).
[6]K. A. Nugent, T. E. Gureyev, D. F. Cookson, D. Paganin, and Z. Barnea, Phys. Rev. Lett. **77**, 2961 (1996).
[7]D. Chapman, W. Thomlinson, R. E. Johnston, D. Washburn, E. Pisano, N. Gmür, Z. Zhong, R. Menk, F. Arfelli, and D. Sayers, Phys. Med. Biol. **42**, 2015 (1997).
[8]F. Pfeiffer, T. Weitkamp, O. Bunk, and C. David, Nat. Phys. **2**, 258 (2006).
[9]F. Pfeiffer, M. Bech, O. Bunk, P. Kraft, E. F. Eikenberry, C. Brönnimann, C. Grünzweig, and C. David, Nat. Mater. **7**, 134 (2008).
[10]Z.-F. Huang, K.-J. Kang, L. Zhang, Z.-Q. Chen, F. Ding, Z.-T. Wang, and Q.-G. Fang, Phys. Rev. A **79**, 013815 (2009).
[11]M. Stampanoni, Z. Wang, T. Thüring, C. David, E. Roessl, M. Trippel, R. A. Kubik-Huch, G. Singer, M. K. Hohl, and N. Hauser, Invest. Radiol. **46**, 801 (2011).
[12]I. Zanette, M. Bech, A. Rack, G. Le Duc, P. Tafforeau, C. David, J. Mohr, F. Pfeiffer, and T. Weitkamp, Proc. Natl. Acad. Sci. U.S.A. **109**, 10199 (2012).
[13]T. Thuering, R. Guggenberger, H. Alkadhi, J. Hodler, M. Vich, Z. Wang, C. David, and M. Stampanoni, Skeletal Radiol. **42**, 827 (2013).
[14]P. R. Munro, K. Ignatyev, R. D. Speller, and A. Olivo, Proc. Natl. Acad. Sci. U.S.A. **109**, 13922 (2012).
[15]P. R. Munro, L. Rigon, K. Ignatyev, F. C. Lopez, D. Dreossi, R. D. Speller, and A. Olivo, Opt. Express **21**, 647 (2013).
[16]A. Olivo and R. Speller, Phys. Med. Biol. **52**, 6555 (2007).
[17]P. R. T. Munro, K. Ignatyev, R. D. Speller, and A. Olivo, Opt. Express **18**, 19681 (2010).
[18]E. Pagot, P. Cloetens, S. Fiedler, A. Bravin, P. Coan, J. Baruchel, J. Härtwig, and W. Thomlinson, Appl. Phys. Lett. **82**, 3421 (2003).
[19]L. Rigon, H.-J. Besch, F. Arfelli, R.-H. Menk, G. Heitner, and H. Plothow-Besch, J. Phys. D **36**, A107 (2003).
[20]M. N. Wernick, O. Wirjadi, D. Chapman, Z. Zhong, N. P. Galatsanos, Y. Yang, J. G. Brankov, O. Oltulu, M. A. Anastasio, and C. Muehleman, Phys. Med. Biol. **48**, 3875 (2003).
[21]D. Pelliccia, L. Rigon, F. Arfelli, R.-H. Menk, I. Bukreeva, and A. Cedola, Opt. Express **21**, 19401 (2013).
[22]A. Bravin, P. Coan, and P. Suortti, Phys. Med. Biol. **58**, R1 (2013).
[23]A. Olivo, F. Arfelli, G. Cantatore, R. Longo, R. H. Menk, S. Pani, M. Prest, P. Poropat, L. Rigon, G. Tromba, E. Vallazza, and E. Castelli, Med. Phys. **28**, 1610 (2001).
[24]A. Olivo and R. Speller, Appl. Phys. Lett. **91**, 074106 (2007).
[25]A. Olivo and R. Speller, Phys. Med. Biol. **53**, 6461 (2008).
[26]P. R. Munro, K. Ignatyev, R. D. Speller, and A. Olivo, Opt. Express **18**, 4103 (2010).
[27]M. Born and E. Wolf, *Principles of Optics* (Cambridge Univ. Press, 1999).
[28]L. Rigon, F. Arfelli, and R.-H. Menk, J. Phys. D **40**, 3077 (2007).
[29]Y. I. Nesterets, Opt. Commun. **281**, 533 (2008).
[30]W. Yashiro, Y. Terui, K. Kawabata, and A. Momose, Opt. Express **18**, 16890 (2010).
[31]S. V. Gasilov and P. Coan, J. Opt. Soc. Am. A **29**, 1870 (2012).
[32]A. Olivo, S. Gkoumas, M. Endrizzi, C. K. Hagen, M. B. Szafraniec, P. C. Diemoz, P. R. T. Munro, K. Ignatyev, B. Johnson, J. A. Horrocks, S. J. Vinnicombe, J. L. Jones, and R. D. Speller, Med. Phys. **40**, 090701 (2013).
[33]See supplementary material at http://dx.doi.org/10.1063/1.4861855 for discussion on the efficacy of the method in comparison with conventional absorption imaging.
[34]N. Perry, M. Broeders, C. de Wolf, and S. Toernberg, *European Guidelines for Quality Assurance in Mammography Screening*, 3rd ed. (European Commission, Luxembourg, 2001).
[35]T. P. Millard, M. Endrizzi, K. Ignatyev, C. K. Hagen, P. R. T. Munro, R. D. Speller, and A. Olivo, Rev. Sci. Instrum. **84**, 083702 (2013).
[36]A. Olivo, K. Ignatyev, P. R. T. Munro, and R. D. Speller, Appl. Opt. **50**, 1765 (2011).
[37]K. Ignatyev, P. R. T. Munro, D. Chana, R. D. Speller, and A. Olivo, J. Appl. Phys. **110**, 014906 (2011).
[38]G. Harding, Radiat. Phys. Chem. **71**, 869 (2004).
[39]V. Revol, I. Jerjen, C. Kottler, P. Schütz, R. Kaufmann, T. Lüthi, U. Sennhauser, U. Straumann, and C. Urban, J. Appl. Phys. **110**, 044912 (2011).
[40]T. Kunisada, D. Shimao, H. Sugiyama, K. Takeda, T. Ozaki, and M. Ando, Eur. J. Radiol. **68**, S18 (2008).
[41]M. Fernández, J. Keyriläinen, R. Serimaa, M. Torkkeli, M.-L. Karjalainen-Lindsberg, M. Leidenius, K. von Smitten, M. Tenhunen, S. Fiedler, A. Bravin, T. M. Weiss, and P. Suortti, Phys. Med. Biol. **50**, 2991 (2005).
[42]T. Michel, J. Rieger, G. Anton, F. Bayer, M. W. Beckmann, J. Durst, P. A. Fasching, W. Haas, A. Hartmann, G. Pelzer, M. Radicke, C. Rauh, A. Ritter, P. Sievers, R. Schulz-Wendtland, M. Uder, D. L. Wachter, T. Weber, E. Wenkel, and A. Zang, Phys. Med. Biol. **58**, 2713 (2013).